Spatio-temporal development of the pairing instability in an infinite array of vortex rings

2014 Fluid Dyn. Res. 46 061405

(http://iopscience.iop.org/1873-7005/46/6/061405)

IOP Publishing | The Japan Society of Fluid Mechanics Fluid *Dynamics* Research

Fluid Dyn. Res. **46** (2014) 061405 (13pp) doi:10.1088/0169-5983/46/6/061405

Spatio-temporal development of the pairing instability in an infinite array of vortex rings

H Bolnot[1,2], S Le Dizès[1] and T Leweke[1]

[1] Aix Marseille University, CNRS, Centrale Marseille, IRPHE UMR 7342, Marseille, 13384, France
[2] Aerodynamics Department, Airbus Helicopters, Marignane, 13725, France

E-mail: ledizes@irphe.univ-mrs.fr

Received 29 August 2013, revised 11 April 2014
Accepted for publication 17 April 2014
Published 3 October 2014

Communicated by Y Fukumoto

Abstract

In this paper, we study the linear stability of an infinite vortex ring array with respect to the pairing instability, using a spectral code. The base flow solution, obtained after a short relaxation process, is composed of rings with a Gaussian azimuthal vorticity profile. The temporal stability properties are first obtained and compared to the theoretical predictions obtained by Levy and Forsedyke (1927 *Proc. R. Soc. Lond.* A **114** 594–604). The spatio-temporal evolution of a localized perturbation is then computed. The growth rate $\sigma(v)$ of the perturbation in the frame moving at the speed v is obtained for all v. The variation of $\sigma(v)$ with respect to the parameters of the flow is provided.

(Some figures may appear in colour only in the online journal)

1. Introduction

Vortex pairing is a process occurring in arrays of identical concentrated vortices, whereby small perturbations of their initially equidistant positions are amplified in such a way that neighboring vortices approach each other and group in pairs. It occurs, for example, in shear layers, as a secondary instability of the Kelvin-Helmholtz instability (Winant and Browand 1974). Pairing is distinct from merging of two vortex cores of like-signed vorticity into a single one, which occurs when the two initial vortices come sufficiently close to each other (see, for example, Meunier *et al* 2005). Merging may take place during the late stages of the pairing instability in arrays of real (distributed) vortices.

The pairing instability has been mainly studied in a two-dimensional (2D) framework for infinite arrays of straight vortices. Von Kármán (1912) analyzed the stability of various arrangements of point vortices. He found that single arrays, double symmetric or alternate

arrays were all unstable whatever the spacing between the vortices. Interestingly, he found a same maximum growth rate for all cases, equal to $\sigma = \pi\Gamma/\left(4\,h^2\right)$ where Γ is the circulation of the vortices and h the vortex spacing along the array (Lamb 1932). Pierrehumbert and Widnall (1982) and Brancher and Chomaz (1997) studied the effect of a finite core size in a single array by considering the exact solution obtained by Stuart (1967). Pierrehumbert and Widnall (1982) showed that the array could also be unstable with respect to three-dimensional (3D) perturbations. Brancher and Chomaz (1997) analyzed the spatio-temporal development of the pairing instability and described its absolute/convective character.

3D configurations were less studied, mainly due to the lack of analytic base flow solutions. Levy and Forsdyke (1927) used a filament approach to analyze the stability of an infinite array of ring vortices. It will be shown here that their results, obtained in the limit of small core size, provide a good approximation of the numerical stability properties in a large range of parameters.

The pairing instability is also expected to occur in the context of helical vortices formed in the wake of wind turbines (Alfredsson and Dahlberg 1979), propellers (Felli *et al* 2011) or helicopter rotors (Leishman 2006). Using a filament approach, Widnall (1972) predicted the existence of instabilities in a single helical vortex. These instabilities are related to the 2D pairing instability, as they possess a comparable growth rate. Widnall's work was further extended to the case of multiple interlaced helical vortices by Gupta and Loewy (1974) and Okulov (2004). Recent experiments and simulations attempt to evidence these instabilities in realistic helical wakes (see Walther *et al* 2007, Ivanell *et al* 2010, Leweke *et al* 2013).

Since realistic wakes are (weakly) spatially developing, the stability properties obtained for an infinite array of identical vortices, or for uniform helical vortices, can only be considered as 'local'. The ideas developed by Huerre and Monkewitz (1990) have to be used to connect the observed global behavior to the local stability properties of the wake. As explained by Huerre and Monkewitz (1990), the ability of the perturbations to grow at the place where they are generated (absolute instability) instead of being advected (convective instability) is of particular interest, as this local property is often the signature of a global transition of the flow. For instance, both the transition to the periodic regime in a cylinder wake (Hammond and Redekopp 1997) and the transition to dripping in a capillary jet (Le Dizès 1997) have been associated with the appearance of a region of absolute instability in the flow. We suspect that the so-called vortex ring state (VRS) transition (MeijerDrees and Hendal 1951), which is observed in the steep-descent regimes of helicopters, could be interpreted in a similar way, and be related to the transition from convective to absolute of the pairing instability of the vortices generated by the helicopter rotor blades. The present study, which fully characterizes the convective/absolute nature of the pairing instability in a simplified axisymmetric model of a rotor wake, can then be considered as the first building block of a global theory explaining the VRS transition.

The paper is organized as follows. In section 2, the numerical tool and the flow parameters are introduced. In section 3, we describe the base flow solution and its properties. In section 4, we first perform a temporal stability analysis of the pairing instability and compare our results to the theoretical predictions of Levy and Forsdyke (1927). Then, a spatio-temporal stability analysis is carried out following the approach of Brancher and Chomaz (1997). The results are compared to the predictions obtained for point vortices.

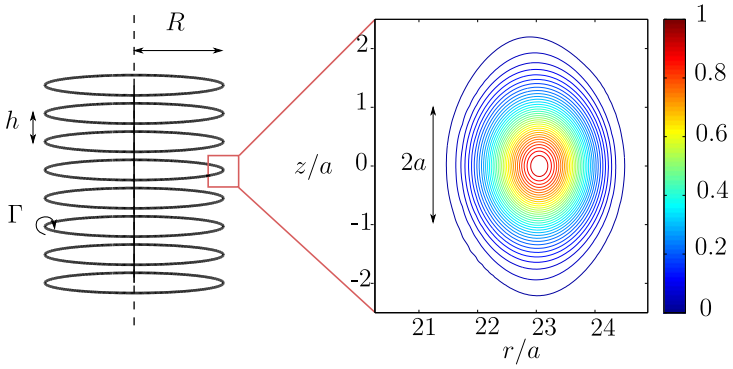

Figure 1. Schematic representation of a vortex ring array and associated azimuthal vorticity contours (in the (r, z) plane), computed by DNS for $R/a = 23$ and $h/a = 6.4$ at $Re = 2000$.

2. Framework

2.1. Description of the flow

We consider as base flow an infinite array of identical axisymmetric vortex rings of circulation Γ, radius R and core size a, separated by a distance h in an incompressible fluid of kinematic viscosity ν (see figure 1). The azimuthal vorticity profile of each ring is chosen to be Gaussian, so the base flow is mainly characterized by the two scale ratios R/a and h/a, and the Reynolds number $Re = \Gamma/(2\pi\nu)$ of the system. The Reynolds number is assumed large, so that the time evolution of the system associated with viscous diffusion can be neglected. In practice, we freeze the base flow after a short relaxation process, needed to obtain a quasi-steady solution, in order to perform the stability calculation. The parameters R/a and h/a are assumed larger than 2, so that most of the vorticity remains confined within each vortex ring. The stability of the base flow is analyzed in a frame of reference where the fluid is at rest at infinity. We shall use as a characteristic spatial scale the separation distance h, and as a characteristic time scale $\tau = \Gamma/(2\,h^2)$. As shown below, this time scale is related to the time needed for the ring array to travel the distance h by its self-induced motion. In the following, dimensionless variables are noted with a star.

2.2. Numerical details

In all the simulations, the flow is assumed to remain axisymmetric. It is governed by the Navier-Stokes equations, which are written for the azimuthal vorticity and streamfunction in a cylindrical domain (r, θ, z). The spatial domain is discretized using a pseudo-spectral method. In the axial direction, a Fourier formulation with equally spaced collocation points is used, in order to ensure periodic boundary conditions. In the radial direction, a Chebyshev polynomial formulation, together with a nonlinear mapping from $(-1, 1)$ to $(-\infty, +\infty)$, is used. As in Antkowiak (2005), the parity properties of the Chebyshev polynomials are taken into account to limit the Chebyshev domain to $(0, 1)$ and easily implement the boundary conditions at the origin and at infinity. The nonlinear mapping, which is typically of the form

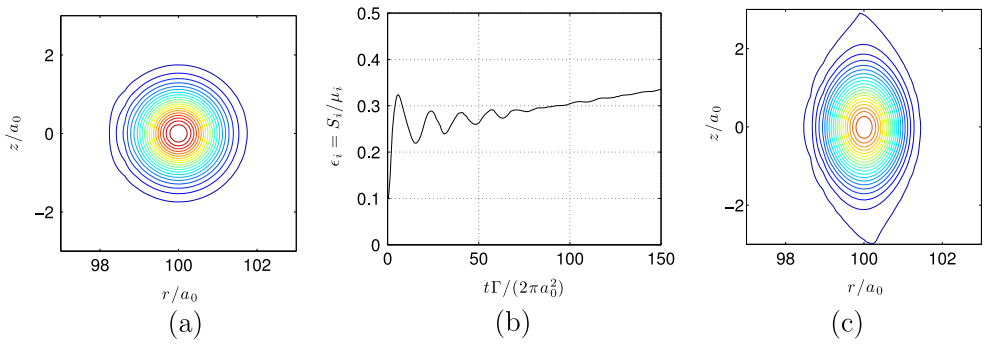

Figure 2. Azimuthal vorticity contours of a vortex ring (a) at initial time and (c) after the relaxation process at time $t\Gamma/\left(2\pi a_o^2\right) = 90$. (b) The corresponding evolution of the local ellipticity for $R/a_o = 100$, $h/a_o = 6$ and $Re = 2000$.

$$r(s) = \frac{s^3}{1 - s^2} + R \tanh\left(\beta s\right) \tag{1}$$

with $\beta = 7$ for $R/a = 100$, is chosen such that at least 16 radial collocation points are present within the ring core $\left(R - a, R + a\right)$. Typically, 100 points are used in the radial direction and 16 h/a points per period in the axial direction.

The time evolution of the flow is computed using a second-order Adams-Bashforth predictor-corrector algorithm. The same code is used to get the base flow and to analyze its stability. The base flow is obtained by integrating the full nonlinear equations in a box of axial dimension h. The evolution of the perturbation is analyzed by considering the equations linearized around the base flow. Except in section 4.3, where viscous effects are considered, the Reynolds number is fixed to 2000. This value is large enough to guarantee that the viscous diffusion of the vortex rings can be neglected in the perturbation analysis and that the stability characteristics are close to the large Reynolds number limit.

3. Base flow calculation

No analytical solution of an array of vortex rings exists, so the base flow has to be computed numerically. This is possible with the present DNS code, because the pairing instability can be filtered out by considering a small axial domain with only one period. In such a small domain, the imposed periodicity forbids the movement of one ring towards its neighbor, and therefore inhibits the pairing instability.

3.1. Relaxation process

The simulation is started with a single vortex ring of core size a_o and radius R, placed at middle height of a box of size h, as initial condition. A Gaussian profile is chosen for the azimuthal vorticity in the ring:

$$\omega_\theta = \frac{\Gamma}{4\pi a_o} e^{-\left[(r-R)^2+z^2\right]/a_o^2}. \tag{2}$$

During the first instants, the vortex ring deforms owing to the effect of vortex images. As explained by Le Dizès and Verga (2002), this process is a non-viscous relaxation process that

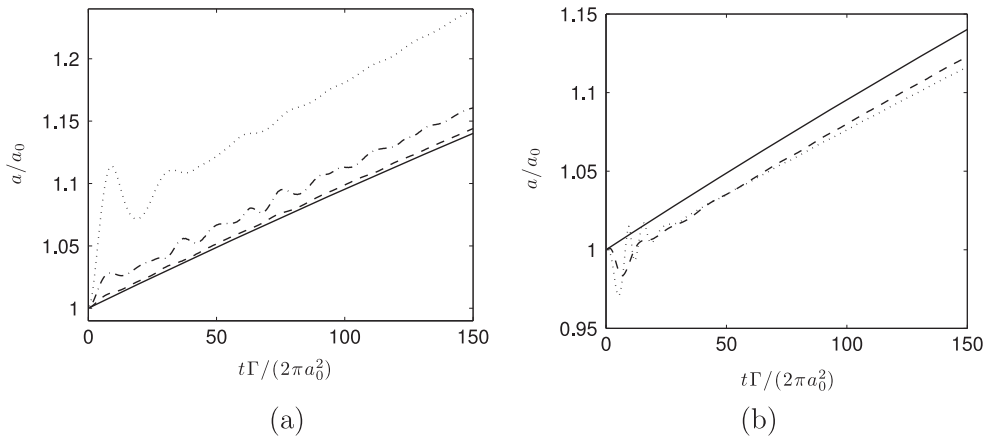

Figure 3. Time evolution of the core size of the vortices ($R/a_o = 100$) measured by (a) the second-order moment of vorticity for $h/a_o = 7$ (dots), 10 (dash-dot) and 15 (dash) and (b) a Gaussian fit of the vorticity field (dash) and the maximum of the azimuthally averaged velocity profile (dots) for $h/a_o = 7$. The viscous evolution, $a = \sqrt{a_o^2 + 4\nu t}$, is plotted in solid lines on both figures.

mainly depends on the initial vorticity profile. For a Gaussian profile, the relaxation process is particularly fast. It can be characterised by plotting the local ellipticity ϵ_i of the streamlines near the vortex center. As shown in figure 2(b), the local ellipticity relaxes to a mean value which evolves on a slower viscous time scale. The relaxed state has typically the form illustrated in figure 2(c): its vorticity contours have been elliptically deformed with a large principal axis aligned with the z-axis when $h < R$. It continues to evolve but on a viscous time scale. The azimuthally averaged vorticity profile in the ring remains Gaussian, and its radius is found not to vary: $R = \mathrm{Cst}$. As long as the vortices are well-separated, the time evolution is mainly associated with the growth of the core size, which follows the viscous law:

$$a(t) = \sqrt{a_o^2 + 4\nu t}\,. \tag{3}$$

3.2. Core size measurement

When the vortex rings are close to each other (small h/a), a small part of the vorticity is advected away, which may affect the measurement of the core size. In figure 3(a), we show that when the core size is computed from the second-order moment of vorticity,

$$a = \sqrt{\frac{\iint \left((r - r_c)^2 + (z - z_c)^2 \right) \omega_\theta \, \mathrm{d}r\mathrm{d}z}{\iint \omega_\theta \, \mathrm{d}r\mathrm{d}z}}\,, \tag{4}$$

where r_c and z_c are, respectively, the radial and axial position of the centroid of vorticity, a departure from the viscous law (3) is observed when $h/a < 15$. The second-order-moment formula tends to overestimate the core size. This effect can be associated with the advection of some vorticity away from the vortex core during the relaxation process. Although the quantity of vorticity (circulation) pulled away is not visible, it has a large impact on the second-order moment. However, the vortex core is almost not modified. Another definition of the core size, which is not affected by events occurring far away from the vortex, could then be more appropriate.

In figure 3(b), we have plotted the evolution of the core size using two other definitions: 1) one involving the position r_{max} of the maximum of the azimuthally averaged azimuthal velocity (using $a = r_{max}/1.12$ for a Gaussian vortex); and 2) the core size obtained from a Gaussian fit of the azimuthally averaged vorticity profile. As observed, these curves are much closer to the viscous prediction than the second-order moment curve. They are both below the theoretical prediction, which is not surprising since some vorticity has been stripped away. Note, however, that the difference remains smaller than 2%. In the following, we shall use the viscous prediction to estimate the core size of the vortex after the relaxation process. The above consideration demonstrates that this provides a reasonable estimate of the core size.

3.3. Advection speed

The fluid is at rest at infinity, but the vortex ring array is moving at constant speed in the axial direction. This advection velocity mainly depends on the geometrical characteristics h/a and R/a of the system. Using an inviscid filament approach, Levy and Forsdyke (1927) provided an expression for the advection speed of the form $v_{adv} = U + V$, where U is the self-induced velocity of a single vortex ring and V is the velocity induced by all the other rings:

$$U = \frac{\Gamma}{4\pi R}\left(\ln\frac{8R}{a_R} - \frac{1}{4}\right), \tag{5}$$

$$V = \frac{\Gamma}{4\pi R}\sum_{n=1}^{\infty}\alpha_k\left[\mathbf{K}\left(\alpha_k^2\right) - \mathbf{E}\left(\alpha_k^2\right)\right]. \tag{6}$$

In (6), $\mathbf{K}$ and $\mathbf{E}$ are the complete elliptic integrals of first and second kind, respectively (Abramowitz and Stegun 1970), and $\alpha_k = \left[1 + \left(kh\right)^2/\left(2R\right)^2\right]^{-1/2}$. The self-induced velocity U depends on the rings' vorticity profile. The above expression is valid for rings with constant vorticity (Rankine vortex of radius a_R). As shown by Widnall *et al* (1971), this expression can be modified to account for a different vorticity profile and the presence of an axial flow, by replacing a_R by an equivalent core size a_e defined by

$$a_e = a \cdot e^{1/4 - X + Y}, \tag{7}$$

where a is a characteristic variation length scale for the azimuthal and axial velocity fields v_ϕ and v_x within the vortex, and

$$X = \lim_{\rho\to\infty}\left[\frac{4\pi^2}{\Gamma^2}\int_0^\rho \bar{r}v_\phi^2(\bar{r})\,\mathrm{d}\bar{r} - \ln\frac{\rho}{a}\right] \quad \text{and} \quad Y = \frac{8\pi^2}{\Gamma^2}\int_0^\infty \bar{r}v_x^2(\bar{r})\,\mathrm{d}\bar{r}. \tag{8}$$

We recover $a_e = a_R$ for a Rankine vortex and obtain $a_e \approx 1.36a$ for a Gaussian vortex with a defined by (4) (Leweke and Williamson 2011). This leads, for a Gaussian vortex without axial flow, to the expression given in Saffman (1992) for the induced velocity:

$$U = \frac{\Gamma}{4\pi R}\left(\ln\frac{8R}{a} - 0.558\right). \tag{9}$$

This expression is used in the following.

When both R/h and R/a are large, the advection velocity reduces to $v_{adv} \sim \Gamma/\left(2\,h\right)$ which is the value obtained for a double row of straight identical vortices (Von Kármán 1912). In figure 4, we compare the advection velocity computed numerically with the theoretical predictions. As expected, we observe that Levy and Forsdyke's formula provides a good

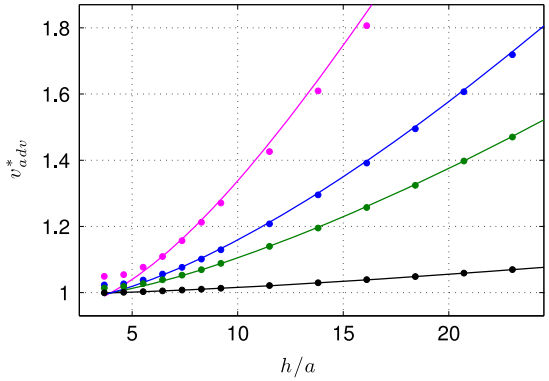

Figure 4. Advection speed $v^*_{adv} = v_{adv} \cdot \left(2\,h/\Gamma\right)$ of a vortex ring array as a function of the vortex spacing for radii $R/a \simeq 4.6$, 9.2, 13.8 and 92.1 (from top to bottom). Theoretical predictions (lines) of Levy and Forsdyke (1927) and numerical calculations (♦) at $Re = 2000$.

estimate of v_{adv} when h/a and R/a become large. We also note that the 2D limit is recovered for the largest R/a.

4. Stability analysis

In this section, we analyze the evolution of linear perturbations to the base flow obtained in the previous section. As mentioned above, for this purpose, the Navier-Stokes are linearized around a base flow frozen after the end of the relaxation process. The weak diffusion of the base flow is then neglected and therefore, in the frame moving at the advection speed of the rings, the base flow solution is stationary. This simplification guarantees that perturbations can be sought in the form of temporal modes (proportional to $e^{i\omega t}$, where ω is a complex frequency), and that we can define a maximum growth rate $\sigma_{\max} = \max\left[-\mathrm{imag}\left(\omega\right)\right]$. This simplification is also justified on a physical ground, since our goal is to apply the results to flows with a much larger Re, where viscous diffusion is indeed negligible. Note, however, that we still include the effect of viscous diffusion on the perturbations, but this effect is small for $Re = 2000$, because of the inviscid nature of the pairing instability. We first consider the temporal stability characteristics by searching the most unstable temporal normal mode. Then, we analyze the spatio-temporal development of the perturbations by considering a localized initial perturbation.

4.1. Temporal evolution

The temporal stability of an infinite vortex ring array has been studied theoretically by Levy and Forsdyke (1927) using a filament approach. They have obtained a formula for the growth rate of the pairing instability for uniform-vorticity rings. This formula is given in appendix A, together with a more general expression to account for a different vortex profile and the presence of vortex stretching.

The theoretical formula for the pairing instability growth rate is plotted and compared to the numerical results in figure 5. The latter are obtained by considering the time evolution of perturbations initiated for a white-noise initial condition in a box of height $2h$. At sufficiently large time, the most unstable mode corresponding to the pairing instability emerges, and its

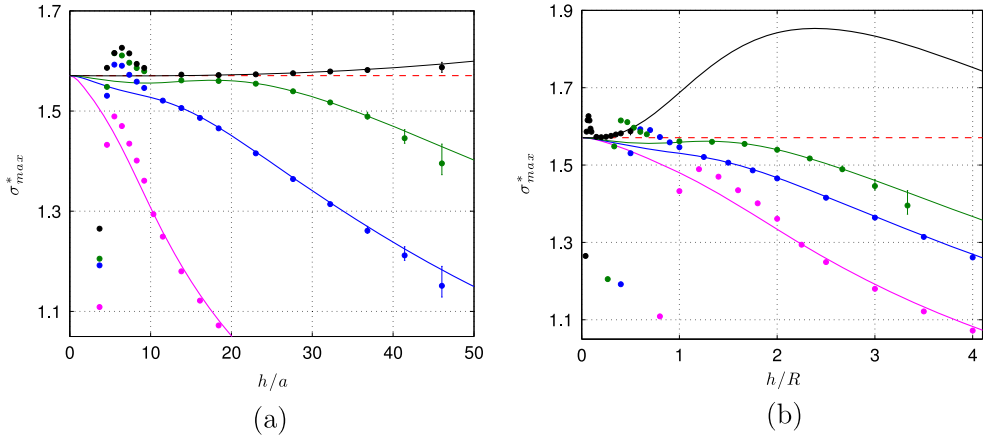

Figure 5. Comparison of the temporal growth rates calculated by Levy and Forsdyke (1927) (solid lines) and the numerical simulations (symbols) for $R/a = 4.6$, 9.2, 13.8 and 92.1 (from bottom to top), as a function of (a) h/a and (b) h/R. The dashed red line represents the 2D point vortex prediction $\sigma^*_{\max} = \pi/2$.

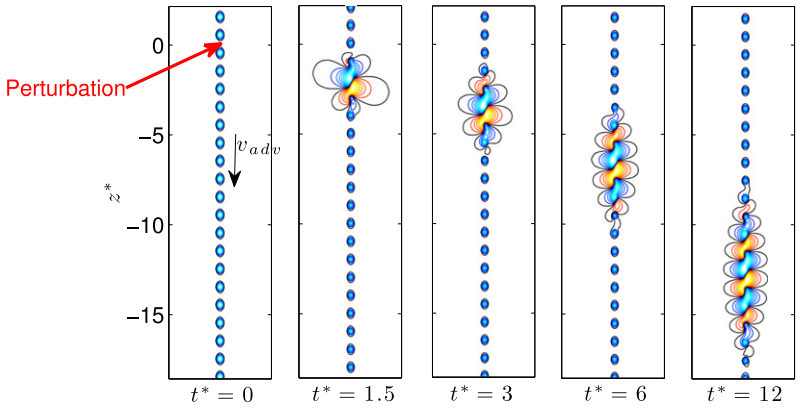

Figure 6. Vorticity contours of the linear perturbation superimposed on the base flow, as a function of time $t^* = t\Gamma/(2\,h^2)$ for $h/a = 6$, $R/a = 92.1$ and $Re = 2000$. The amplitude of the perturbation is renormalized in each plot for presentation purposes.

growth rate can easily be estimated. The maximum growth rates are plotted as functions of h/a and h/R in figure 5. In figure 5(a), we observe good agreement between the numerical and analytical predictions for $h/a > 10$. For $4 < h/a < 10$, there is a visible effect of the core size: the theoretical predictions systematically underestimate the numerical results. When $h/a < 4$, a strong fall of the numerical growth rate is observed. This behavior may be not relevant, since the base flow never really reaches a quasi-stationary state for such small values of h/a. It is worth mentioning that for small h/R Levy and Forsdyke's prediction is very close to the 2D prediction $\sigma^* = \pi/2$ obtained for point vortices. This 2D result therefore provides a very good estimate of the numerical growth rate for large R/a (typically $R/a > 25$), if h/R is smaller than 0.5. This is important for applications involving helicopter or wind turbine wakes, which are typically in this range of parameters.

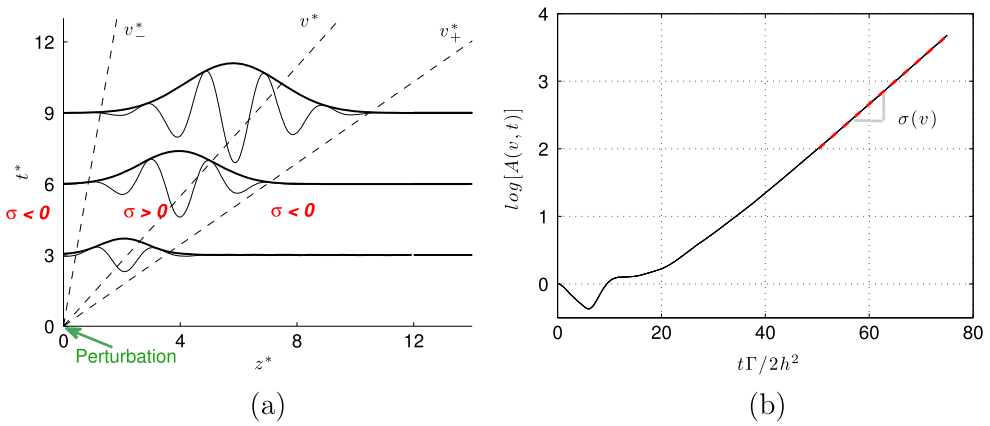

Figure 7. (a) Spatio-temporal evolution of the axial velocity perturbation $u_z(r, z)$ and its envelope (bold lines) at $r = R$ as a function of the axial coordinate ($z^* = z/h$) and time ($t^* = t\Gamma/(2h^2)$) for $h/a = 4.6$, $R/a = 92.6$ and $Re = 2000$. (b) Example of the amplitude evolution for a particular value of v^*, represented on a log scale for graphical convenience.

4.2. Spatio-temporal evolution

In order to analyze the spatio-temporal development of the perturbations, the domain of simulation is extended to at least $30h$ along the axial direction. The simulation is started with a localized initial condition in the form of a Gaussian envelope for the streamfunction perturbation. The size and location of the initial perturbation have been varied. It cannot be made too small, owing to our finite spatial resolution. A good choice was found to be a perturbation of size $a/2$, placed close to the middle point between two rings. Such an initial perturbation gives rise to a wave packet growing in time and in space, as illustrated in figure 6.

From the axial velocity signal, a mean amplitude of the wave packet is extracted along each ray $z^* = v^*t^*$ for a fixed speed v^*, following the procedure used by Brancher and Chomaz (1997). We filter out all axial wavenumbers higher than $2\pi/h$ and use the Hilbert transform to obtain an amplitude at each radial position. A mean amplitude is then obtained by taking the average over all r. As explained by Brancher and Chomaz (1997), this procedure avoids a Floquet analysis and readily provides, after having waited for a sufficiently long time, an amplitude which grows exponentially in time on any ray propagating at a speed between two critical values, v_-^* and v_+^*. A typical evolution of the amplitude in this regime is illustrated in figure 7(b). For each value of $v^* = z^*/t^*$, one obtains a measure of a (temporal) growth rate $\sigma^*(v^*)$. In practice, the simulation is stopped when the wave packet has reached an asymptotic regime but before its width exceeds half the height of the domain in order to avoid mirror effects due to the periodic boundary conditions.

In all cases, the maximum of $\sigma^*(v^*)$ is reached at $v^* \approx 1$ and is close to the maximum temporal growth rate, as expected. The growth rate $\sigma^*(v^*)$ has been obtained as a function of the different parameters (R/a, h/a) of the system. The results are plotted in figure 8(a) for a large ratio $R/a = 92.1$ for different values of h/a. This figure shows that, when the growth rate is normalized using $\Gamma/(2h^2)$, $\sigma^*(v^*)$ becomes almost independent of h/a for $h/a > 5$.

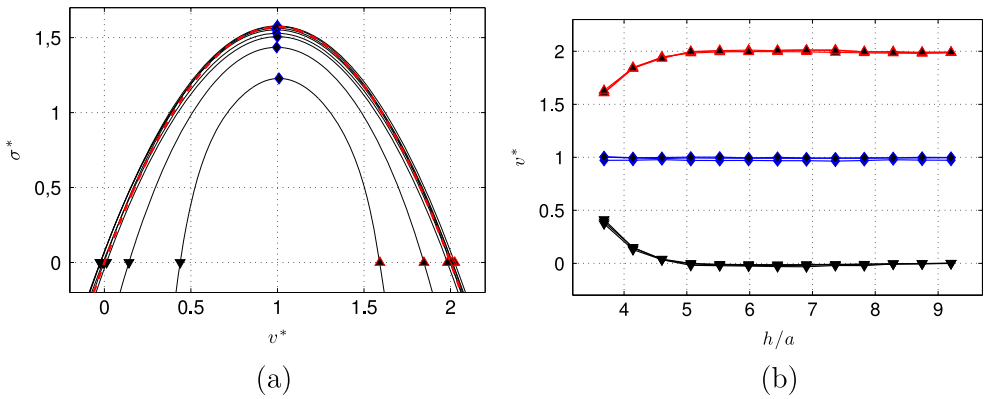

Figure 8. (a): Growth rate of the wave packet envelope as a function of the group velocity v^* for $h/a \simeq 4, 5, 7, 8, 10$, at $R/a = 92.1$ and $Re = 2000$. The analytical prediction for straight vortices in the two-dimensional case (equation (12)) is plotted with a red dashed line. (b) Values of v_-^* (▼), v_+^* (▲) and $v^*_{\sigma^*=\sigma^*_{max}}$ (♦) versus h/a for $R/a = 13.8, 46, 92.1$.

For small values of h/a, the growth rate becomes significantly smaller. For the smallest value that we were able to consider ($h/a \approx 3.7$), the vortices are so close that they almost form a shear layer. The dashed red line in figure 8(a) represents the theoretical prediction for a double array of point vortices, which corresponds to the limit of large R/a and large R/h. As written in Lamb (1932) [section 156], the dispersion relation for 2D perturbations of wavenumber k in such a flow is given by:

$$\sigma_{2D}(k) = \frac{\Gamma}{2h}\, k\left(1 - \frac{kh}{2\pi}\right) \tag{10}$$

As explained by Huerre and Monkewitz (1990), the growth rate of the wave packet moving at the group velocity v is then given by $\sigma_{2D}\left(k_o(v)\right)$, where $k_o(v)$ is defined by

$$\frac{\partial \sigma_{2D}}{\partial k}\left(k_o\right) = v. \tag{11}$$

In terms of our non-dimensional variables, we then obtain:

$$\sigma^*_{2D}\left(v^*\right) = \frac{\pi}{2} v^*\left(2 - v^*\right). \tag{12}$$

As observed in figure 8(a), this theoretical prediction provides a very good estimate of the numerical results. Note in particular that for $h/a \geqslant 7$, the critical speeds v_-^* and v_+^* of the wavepacket are very well predicted by the point vortex theory: the rear of the wave packet stays in the vicinity of the initial perturbation location, whereas the front propagates at about twice the characteristic convection speed.

The variation of v_-^*, v_+^* and $v^*_{\max}$ with h/a is shown for different values of the ratio R/a in figure 8(b). We note that R/a has to be of order 5 or smaller to observe any effect. As mentioned above, the instability is weaker for small values of h/a, so v_-^* increases and v_+^* decreases.

In the absolute/convective terminology (Huerre and Monkewitz 1990), the results can be interpreted as follows. In any frame moving at a speed within the interval $\left(v_-^*, v_+^*\right)$, the

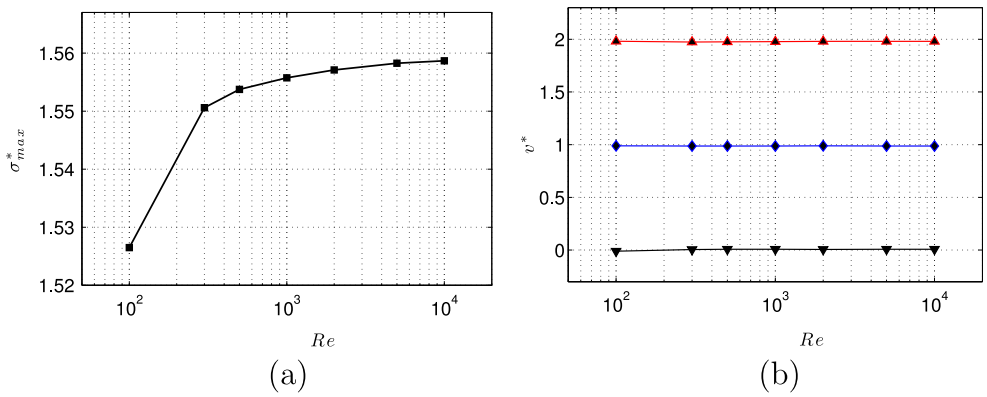

Figure 9. Evolution of (a) the maximum growth rate $\sigma^*_{\max}$ and (b) velocities v_-^* (▼), v_+^* (▲) and $v^*_{\sigma^*=\sigma^*_{max}}$ (♦) as a function of the Reynolds number for $h/a = 6$ and $R/a = 46$.

wavepacket grows at the place it has been created, the instability is therefore absolute. In the other cases, the wavepacket moves away as it grows, the instability is convective.

4.3. Reynolds number effects

In the previous sections, the Reynolds number was fixed at a value of 2000. In this section, the effect of viscosity on the stability results is assessed. The results are summarized in figure 9. In figure 9(a), we see that the maximum temporal growth rate is less than 1% from the inviscid limit for $Re > 300$. In figure 9(b), no visible effect on the three characteristic velocities v_-^*, v_+^* and $v^*_{\max}$ is observed as the Reynolds number is varied from Re between 100 and 2000. These plots have been obtained for a given set of parameters. We have tried other values of R/a and h/a and similar observations have been made.

The conclusion is that the dependence on the Reynolds number of the stability properties becomes negligible for Re above a few hundred. This is not a surprising result, since the mechanism of instability is non-viscous and therefore marginally affected by viscosity when the Reynolds number is sufficiently large. All the results obtained for $Re = 2000$ can be considered as almost inviscid.

5. Conclusion

In this paper, we have analyzed the stability properties of an infinite array of vortex rings with a Gaussian vorticity profile. Finite core sizes have been considered in order to extend previous results obtained by Levy and Forsdyke (1927). We have first considered the base flow and computed the advection velocity of the vortex system for various R/a and h/a. Good agreement with the theoretical results was found for large R/a and h/a. The temporal stability properties of the pairing instability have been computed, and the effect of the different parameters has been analyzed. An effect of the finite core size has been evidenced for small R/a or small h/a. The spatio-temporal development of the pairing instability has also been considered. An important result is that, as soon as R/a is larger than 10 and h/a larger than 7, the development of the instability is almost independent of these parameters when h and $2\,h^2/\Gamma$ are chosen as spatial and temporal scales. In these cases, the growth rate $\sigma^*\left(v^*\right)$ of the

most unstable perturbation along the ray $z^* = v^* t^*$ is very close to the theoretical formula (12) obtained for an array of points vortices. The effect of viscosity has also been analyzed and shown to have no visible impact on the stability properties for $Re > 300$.

Acknowledgments

HB was supported by Airbus Helicopters through a doctoral grant (contract no. IPEC 0187N/2009). This work also received support from the French *Agence Nationale de la Recherche* under the A*MIDEX grant ANR-11-IDEX-0001-02, the LABEX MEC project ANR-11-LABX-0092 and the ANR HELIX project ANR-12-BS09-0023-01.

Appendix. Temporal growth rate expression

In this section, we provide the temporal growth rate formula obtained by Levy and Forsdyke (1927). Using our notation and the normalization by $\Gamma/\left(2\,h^2\right)$, their expression can be written (after having corrected the misprint appearing in their expression of B) as

$$\sigma^* = \frac{h^2}{\pi R^2}\sqrt{C\left(G + C/2 + H_o - B\right)}, \tag{A.1}$$

with

$$B = \sum_{p=1}^{\infty} \frac{\alpha_{2p-1}^3}{2}\left[\left(3 + \beta_{2p-1}^2\right)\mathrm{E}\left(\alpha_{2p-1}^2\right) - \mathrm{K}\left(\alpha_{2p-1}^2\right)\right], \tag{A.2}$$

$$C = \sum_{p=1}^{\infty} \alpha_{2p-1}^3\left[\left(1 - \beta_{2p-1}^2\right)\mathrm{E}\left(\alpha_{2p-1}^2\right) - \mathrm{K}\left(\alpha_{2p-1}^2\right)\right], \tag{A.3}$$

$$G = \sum_{p=1}^{\infty} \alpha_{2p}^3\left[2\mathrm{E}\left(\alpha_{2p}^2\right) - \mathrm{K}\left(\alpha_{2p}^2\right)\right], \tag{A.4}$$

$$\alpha_k = \left[1 + \left(\frac{kh}{2R}\right)^2\right]^{-1/2}; \quad \beta_k = \frac{2R}{kh}. \tag{A.5}$$

The functions K and E are the complete elliptic integrals of the first and second kind, respectively (Abramowitz and Stegun 1970, p. 590). The term H_o is associated with the radial variation of the self-induced velocity of a single ring: $H_o = dU/dR$. Levy and Forsdyke (1927) gave its expression for a ring with a uniform vorticity profile, which in our notation reads

$$H_o = \frac{1}{2}\left(\frac{5}{4} - \ln\frac{8R}{a}\right). \tag{A.6}$$

As mentioned in section 3.3, an expression for U can be obtained for any type of vortices by considering an equivalent radius a_e, as defined by (7). Moreover, the vortex ring is subject to vortex stretching. Therefore a is expected to vary with respect to R as $R^{-1/2}$, in order to conserve the total circulation. This effect was not considered by Levy and Forsdyke (1927). It adds a constant 1/2 in the parenthesis such that

$$H_o = \frac{1}{2}\left(\frac{7}{4} - \ln\frac{8R}{a_e}\right), \tag{A.7}$$

which now takes into account both the change of the vorticity profile and the effect of vortex stretching.

References

Abramowitz M and Stegun I A 1970 *Handbook of Mathematical Functions* (New York: Dover)

Alfredsson P A and Dahlberg J Å 1979 A preliminary wind tunnel study of windmill wake dispersion in various flow conditions *Technical Note AU-1499* Part 7 (Stockholm: The Aeronautical Research Institute of Sweden)

Antkowiak A 2005 Dynamique aux temps courts d'un tourbillon isolé *PhD Thesis* Université Paul Sabatier, Toulouse, France

Brancher P and Chomaz J M 1997 Absolute and convective secondary instabilities in spatially periodic shear flows *Phys. Rev. Lett.* **78** 658–61

Felli M, Camussi R and Di Felice F 2011 Mechanisms of evolution of the propeller wake in the transition and far fields *J. Fluid Mech.* **682** 5–53

Gupta B P and Loewy R G 1974 Theoretical analysis of the aerodynamic stability of multiple, interdigitated helical vortices *AIAA J* **12** 1381–7

Hammond D A and Redekopp L G 1997 Global dynamics of symmetric and asymmetric wakes *J. Fluid Mech.* **331** 231–60

Huerre P and Monkewitz P A 1990 Local and global instabilities in spatially developing flows *Annu. Rev. Fluid Mech.* **22** 473–537

Ivanell S, Mikkelsen R, Sørensen J N and Henningson D 2010 Stability analysis of the tip vortices of a wind turbine *Wind Energy* **13** 705–15

Lamb H 1932 *Hydrodynamics* (Cambridge: Cambridge University Press)

Le Dizès S 1997 Global modes in falling capillary jets *Eur. J. Mech. B/ Fluids* **16** 761–78

Le Dizès S and Verga A 2002 Viscous interactions of two co-rotating vortices before merging *J. Fluid Mech.* **467** 389–410

Leishman J G 2006 *Principles of Helicopter Aerodynamics* (Cambridge: Cambridge University Press)

Levy H and Forsdyke A G 1927 The stability of an infinite system of circular vortices *Proc. R. Soc. Lond.* A **114** 594–604

Leweke T, Bolnot H, Quaranta U and le Dizès S 2013 Local and global pairing in helical vortex systems *Proc. ICOWES2013 Conf.* ed W Z Shen (Copenhagen: DTU) pp 94–101

Leweke T and Williamson C H K 2011 Experiments on long-wavelength instability and reconnection of a vortex pair *Phys. Fluids* **23** 024101

MeijerDrees J and Hendal W P 1951 Airflow patterns in the neighbourhood of helicopter rotors *Aircr. Eng. Aerosp. Tech* **23** 107–11

Meunier P, Le Dizes S and Leweke T 2005 Physics of vortex merging *C. R. Physique* **6** 431–50

Okulov V L 2004 On the stability of multiple helical vortices *J. Fluid Mech.* **521** 319–42

Pierrehumbert R and Widnall S 1982 The two-and three-dimensional instabilities of a spatially periodic shear layer *J. Fluid Mech.* **114** 59–82

Saffman P G 1992 *Vortex Dynamics* (Cambridge: Cambridge University Press)

Stuart J T 1967 On finite amplitude oscillations in laminar mixing layers *J. Fluid Mech.* **29** 417–40

Von Kármán T 1912 Über den Mechanismus des Flüssigkeits- und Luftwiderstandes *Phys. Z.* **13** 49–59

Walther J H, Guénot M, Machefaux E, Rasmussen J T, Chatelain P, Okulov V L, Sørensen J N, Bergdorf M and Koumoutsakos P 2007 A numerical study of the stability of helical vortices using vortex methods *J. Phys. Conf. Series* **75** 012034

Widnall S E 1972 The stability of a helical vortex filament *J. Fluid Mech.* **54** 641–63

Widnall S E, Bliss D B and Zalay A 1971 Theoretical and experimental study of the stability of a vortex pair *Aircraft Wake Turbulence and its Detection* ed J H Olsen, A Goldberg and M Rogers (New York: Plenum) pp 305–38

Winant C D and Browand F K 1974 Vortex pairing: the mechanism of turbulent mixing-layer growth at moderate Reynolds number *J. Fluid Mech.* **63** 237–55